

We are IntechOpen, the world's leading publisher of Open Access books Built by scientists, for scientists

6,900

Open access books available

186,000

International authors and editors

200M

Downloads

Our authors are among the

154

Countries delivered to

TOP 1%

most cited scientists

12.2%

Contributors from top 500 universities



WEB OF SCIENCE™

Selection of our books indexed in the Book Citation Index
in Web of Science™ Core Collection (BKCI)

Interested in publishing with us?
Contact book.department@intechopen.com

Numbers displayed above are based on latest data collected.
For more information visit www.intechopen.com



Applications of Effective Medium Theories in the Terahertz Regime

Maik Scheller¹, Christian Jansen¹, and Martin Koch²

¹*Institute for High-Frequency Technology, Technische Universität Braunschweig
Schleinitzstr. 22, 38106 Braunschweig*

²*Physics Department, Philipps-Universität Marburg
Renthof 5, 35032 Marburg
Germany*

1. Introduction

In recent years, the investigation of composite material systems in the terahertz (THz) regime has drawn a considerable attention from a wide spectrum of scientific areas, for instance the fields of nano-science (Beard et al., 2002), (Hendry et al., 2006) and metamaterials (Levy et al., 2007). The interaction of terahertz waves with a composite system consisting of particles embedded in a host material as illustrated in Fig. 1 can be described by effective material properties and effective medium theories (EMTs) enabling the calculation of the resulting macroscopic permittivity ϵ_R .

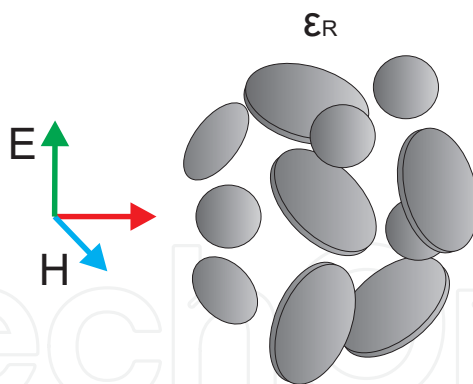


Fig. 1. The interaction between an electromagnetic wave and a composite system can be described by an effective permittivity ϵ_R .

If the particle size is much smaller than the wavelength of interest, as visualized in Fig. 2, scattering effects are negligible and quasi-static models suffice. Otherwise, scattering effects have to be taken into account.

In this book chapter we will review common quasi-static EMTs and their application to various composite material systems. The selection of theoretical models comprises the Landau-Lifshitz-Looyenga model, which is applicable to mixtures of arbitrarily shaped particles, the Polder-van-Santen theory, which explicitly considers the influence of the inclusions shape and orientation, the differential Bruggeman theory and a recent extension to the latter proposed by the authors.

Source: Recent Optical and Photonic Technologies, Book edited by: Ki Young Kim,
ISBN 978-953-7619-71-8, pp. 450, January 2010, INTECH, Croatia, downloaded from SCIYO.COM

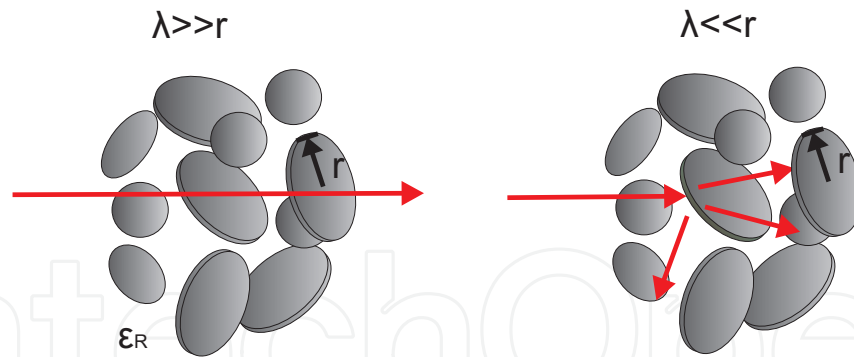


Fig. 2. In the case of small particles compared to the wavelength, quasi-static models suffices, otherwise scattering effects as to be taken into account.

The first application scenario that we will study is the characterisation of polymeric compounds. By adding microscopic particles to a polymeric host material, the resulting properties of the plastic like colour, material strength and flammability can be optimized. Moreover, the additives induce a change of the optical parameters of the mixture that can be studied with terahertz time domain spectroscopy (THz TDS). The resulting refractive index depends on the volumetric content and the dielectric constant of the additives as well as the particle shape. Due to the variety of commonly used additives, ranging from rod like glass fibres, over cellulose based fillers to spherical nanoparticles, polymeric compound systems are ideal to illuminate the applicability and limitations of the different EMTs.

Apart from the polymeric compounds, we will also discuss the usability of the EMTs to describe biological systems. As one example, the water content of plant leaves considerably effects their dielectric properties. Utilizing the EMTs allows for the determination of the water content of the plants with terahertz radiation.

In summary, the chapter will review a selection of effective medium theories and outline their applicability to various scientific problems in the terahertz regime. Additionally, a short overview on the THz time domain spectroscopy (TDS) which is employed to experimentally validate the models' predictions is presented.

2. Effective medium theories

The analysis of dielectric mixture systems, for instance particles embedded in a host material, is a problem of enormous complexity if every single particle is considered individually. Alternatively, the resulting macroscopic material parameter of the mixture can be derived which characterize the interaction between the material system and electromagnetic waves. To calculate this effective material parameter, effective medium theories (EMTs) can be employed. In this chapter, we will exemplarily present a selection of the most common quasi static EMTs which can directly be applied to the description of heterogeneous dielectrics in the THz range. Table 1 provides a basic overview of the characteristics of these models, which will be further described below.

2.1 Maxwell-Garnett

One of the first and probable the most well known EMT is the Maxwell-Garnett (MG) model (Maxwell-Garnett, 1904) which is based on analyzing the effective polarizability of spherical inclusions with the permittivity ϵ_p embedded in a vacuum environment as illustrated in Fig. 3.

| Model | Volumetric content | Particle shape | Area of Application |
|----------------------------|--------------------|----------------|--|
| Maxwell-Garnett | Low | spheres | Very low concentrations |
| Polder and van Santen | High | ellipsoidal | Ellipsoidal particles, anisotropic systems |
| Extended Bruggeman | High | ellipsoidal | High permittivity contrast, ellipsoidal particles, anisotropic systems |
| Landau, Lifshitz, Looyenga | Middle | arbitrary | Mixtures of irregular, unknown shaped particles |
| Complex Refractive Index | middle | arbitrary | Mixtures with small permittivity contrast |

Table 1. Overview of the EMTs mentioned in the text.

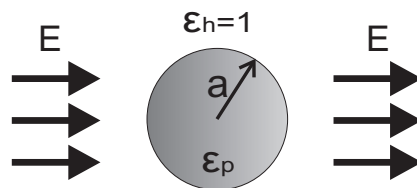


Fig. 3. To derive the MG model, the resulting polarizability of a single spherical particle is derived.

Following the basics of electrostatics the resulting polarizability a_p of a single spherical particle is given by (Jackson, 1999)

$$\alpha_p = 4\pi\epsilon_0 \frac{\epsilon_p - 1}{\epsilon_p + 2} a^3 \quad (1)$$

where ϵ_0 is the permittivity of the vacuum and a is the radius of the particle. Now it is assumed, that the polarizability remains constant if multiple particles are present. Consequently the Clausius Mossoti relation (Kittel, 1995) that connects the relative permittivity ϵ_r of a material with the polarizability of a number of N microscopic particles

$$\frac{\epsilon_r - 1}{\epsilon_r + 2} = \frac{\sum_j N_j \alpha_j}{3\epsilon_0} \quad (2)$$

can be exploited to calculate the effective permittivity ϵ_R of this inhomogeneous medium, where f_p is the volumetric content of the particles:

$$\frac{\epsilon_R - 1}{\epsilon_R + 2} = f_p \frac{\epsilon_p - 1}{\epsilon_p + 2} \quad (3)$$

If the particles are embedded in a host material with given permittivity ϵ_h , Eq. 3 changes into the MG equation:

$$\frac{\epsilon_R - \epsilon_h}{\epsilon_R + 2\epsilon_h} = f_p \frac{\epsilon_p - \epsilon_h}{\epsilon_p + 2\epsilon_h} \quad (4)$$

As can be seen from these deductions, the assumption is violated if a larger volumetric fraction of the medium is formed by the inclusions, since in this case the effective background permittivity changes. Thus, the model can be applied to very low concentrations only.

2.2 Polder and van Santen

Another approach with extended validity was derived by Polder and van Santen: Instead of employing the host ϵ_h in the calculation to derive Eq. 4, the effective dielectric constant ϵ_R is utilized. That way, the effect of the slightly increasing effective background permittivity can be taken into account. The equation

$$\frac{\epsilon_R - \epsilon_h}{3\epsilon_R} = f_p \frac{\epsilon_p - \epsilon_h}{\epsilon_p + 2\epsilon_R} \quad (5)$$

results, which is known as the Böttcher equation (Böttcher, 1942). Despite this extension, the model is still restricted to spherical shaped inclusions. By including depolarization factors N in the deductions, it is possible to expand the validity to ellipsoidal particles. These factors can be calculated by the following equations (Kittel, 1995):

$$N_x = \frac{x_l y_l z_l}{2} \int_0^\infty \frac{du}{(x_l^2 + u) \sqrt{(x_l^2 + u)(y_l^2 + u)(z_l^2 + u)}} \quad (6)$$

$$N_x + N_y + N_z = 1 \quad (7)$$

The Fig. 4 shows the numerically calculated N_x values for different aspect ratios between the axis x and y in a) and the axis x and z in b).

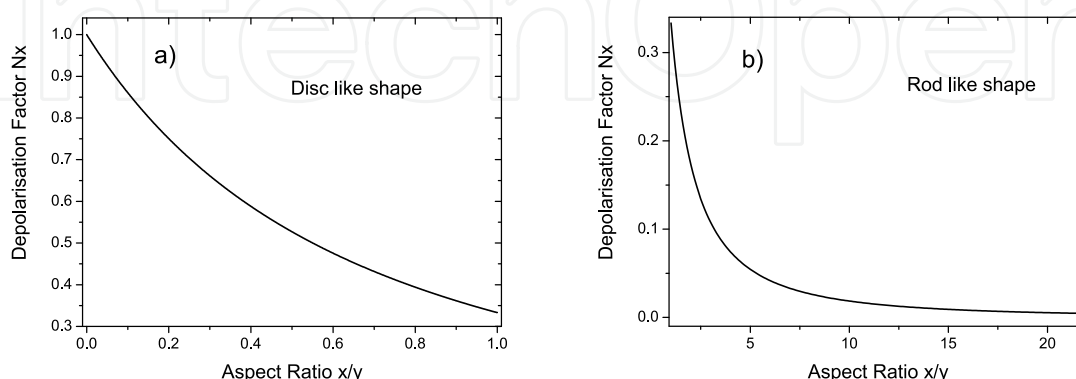


Fig. 4. Values of the depolarisation factor N_x as a function of the aspect ratio between the axis x and y in a) and the axis x and z in b).

In the case of ideal disc-like particles the aspect ratio x/y converges toward zero while the N_x value tends towards unity. For ideal rod like particles, the aspect ratio increase to infinity and N_x descends to zero. These shapes are illustrated together with the resulting depolarization factors in Fig. 5.

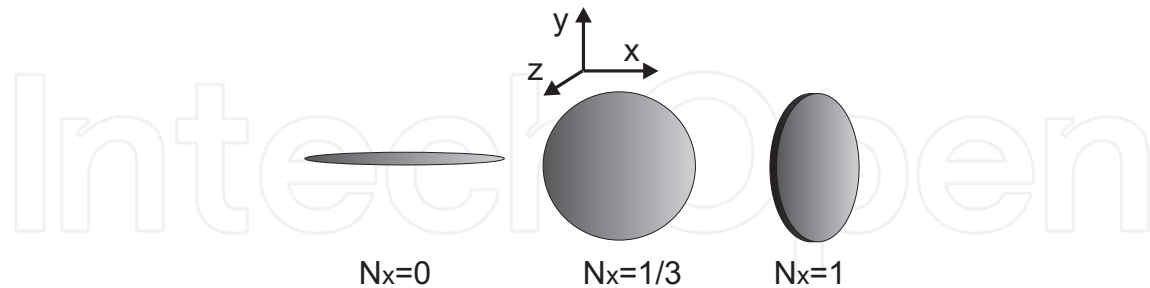


Fig. 5. Values of the depolarisation factor N_x for a) a rod b) a sphere and c) a disc

$$\frac{\epsilon_R - \epsilon_h}{3\epsilon_R} = f_p \frac{\epsilon_p - \epsilon_h}{\epsilon_p + 2\epsilon_R} \quad (5)$$

Analogously to Eq. 5 the effective material parameter can be calculated by employing these factors which results in the Polder and van Santen (PvS) model (Polder & van Santen, 1946):

$$\epsilon_R = \frac{\epsilon_h}{1 - \frac{1}{3} f_p (\epsilon_p - \epsilon_h) \sum_i \frac{1}{\epsilon_R + (\epsilon_p - \epsilon_R) N_i}} \quad (8)$$

The special forms of the PvS model for ideal shapes, which are orientated isotropically in the mixture, are the following (Hale, 1976):

Spheres:

$$\frac{\epsilon_R - \epsilon_h}{3\epsilon_R} = f_p \frac{\epsilon_p - \epsilon_h}{\epsilon_p + 2\epsilon_R} \quad (9)$$

Discs:

$$\frac{\epsilon_R - \epsilon_h}{\epsilon_R + 2\epsilon_p} = f_p \frac{\epsilon_p - \epsilon_h}{3\epsilon_p} \quad (10)$$

Rods:

$$\frac{\epsilon_R - \epsilon_h}{5\epsilon_R + \epsilon_p} = f_p \frac{\epsilon_p - \epsilon_h}{3(\epsilon_p + \epsilon_R)} \quad (11)$$

As the Böttcher model is a special case of the PvS model, the Eq. 9 for spherical shaped particles equals the Böttcher equation Eq. 5.

Due to the consideration of the influence of the particles shape and the increasing background permittivity, the PvS model is widely applicable. Especially anisotropic mixture systems like orientated glass fibres can be described by this approach.

2.3 Bruggeman

While the PvS model well describes a variety of mixtures, a strong contrast in the permittivity between the mixture components still affects its validity. Here, a differential approach (Bruggeman, 1935) can be utilized. The Bruggeman theory makes use of a differential formulation of Eq. 4. After integration, the equation results:

$$1 - f_p = \frac{\varepsilon_p - \varepsilon_R}{\varepsilon_p - \varepsilon_h} \sqrt[3]{\frac{\varepsilon_h}{\varepsilon_R}} \quad (12)$$

which is the basic form of the Bruggeman model. This basic form describes spherical particles embedded in a host where a large contrast in permittivity occurs.

By combining the two approaches (Bruggeman and PvS), more general forms of this model can be derived (Banhegyi 1986), (Scheller et al., 2009, a). The equation for this extended Bruggeman [EB] model in the general case, where one polarization factor is given by N , the other two by $1-N/2$ is:

$$f_p = 1 - \left(\frac{\varepsilon_h}{\varepsilon_R} \right)^{\left[\frac{-3N^2 + 3N}{3N+1} \right]} \left(\frac{\varepsilon_p - \varepsilon_R}{\varepsilon_p - \varepsilon_h} \right) \left(\frac{(1+3N)\varepsilon_p + (5-3N)\varepsilon_h}{(1+3N)\varepsilon_p + (5-3N)\varepsilon_R} \right)^{\left[\frac{12N-18N^2-2}{9N^2-12N-5} \right]} \quad (13)$$

For the case of isotopically orientated particles with ideal shapes the following set of equations results:

Spheres:

$$\frac{\varepsilon_R - \varepsilon_h}{3\varepsilon_R} = f_p \frac{\varepsilon_p - \varepsilon_h}{\varepsilon_p + 2\varepsilon_R} \quad (14)$$

Discs:

$$1 - f_p = \left(\frac{\varepsilon_p - \varepsilon_R}{\varepsilon_p - \varepsilon_h} \right) \left(\frac{2\varepsilon_p + \varepsilon_h}{2\varepsilon_p + \varepsilon_R} \right) \quad (15)$$

Rods:

$$1 - f_p = \left(\frac{\varepsilon_p - \varepsilon_R}{\varepsilon_p - \varepsilon_h} \right) \left(\frac{5\varepsilon_h + \varepsilon_p}{5\varepsilon_R + \varepsilon_p} \right)^{\left[\frac{2}{5} \right]} \quad (16)$$

2.4 Landau, Lifshitz, Looyenga

Additionally, the Landau, Lifshitz, Looyenga (LLL) model (Looyenga 1965) makes use of a different assumption: Instead of taking the shape of the particles into account a virtual sphere is considered, which includes a given volumetric fraction of particles with unknown shape as illustrated in Fig. 3. By successively adding an infinitesimal amount of particles, the effective permittivity increases slightly which can be described by a Taylor approximation. This procedure leads to the equation.

$$\sqrt[3]{\varepsilon_R} = f_p \sqrt[3]{\varepsilon_p} + (1 - f_p) \sqrt[3]{\varepsilon_h} \quad (17)$$

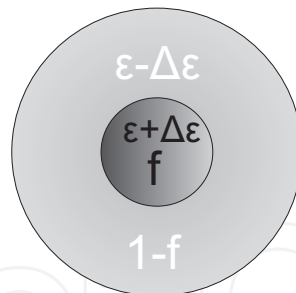


Fig. 3. The basic principle of the LLL model: A given volumetric fraction of particles are embedded in a virtual sphere. By differentially increasing the volumetric fraction f , a Taylor approximation can be utilized to calculate the resulting permittivity ϵ_R of the system.

Here, no shape dependency is taken into account and thus, the model is favourably applicable to irregularly shaped particle mixtures (Nelson 2005).

2.5 Complex Refractive Index (CRI)

Besides from these deductive models, several more empirical approaches exist. The most common one is the Complex Refractive Index (CRI) model, that linearly connects the material parameter to the volumetric content resulting in the equation:

$$n = f_p n_p + (1 - f_p) n_h \quad (18)$$

This model was successfully applied to porous pressed plastics where irregularly shaped air gaps occur and a low permittivity contrast results (Nelson 1990).

3. Terahertz time domain spectroscopy

Terahertz time domain spectroscopy is a relatively young field of science. Apart from some early explorations (Kimmitt, 2003), for a long time the terahertz domain remained a most elusive region of the electromagnetic spectrum. This circumstance can be explained by the lack of suitable sources: while for long the high-frequency operation limit of electronic devices was found in the lower GHz regime, most optical emitters are not able to operate at the "low" THz frequencies.

Many researchers date the advent of nowadays THz science back to the upcoming of femtosecond laser systems (Moulton, 1985). Their short optical pulses could induce carrier dynamics on the timescale of a picosecond, which lead to the development of different broadband THz sources (Kuebler et al., 2005).

Due to the scope of this chapter, the following section will only discuss one of many different ways to generate broadband terahertz radiation, namely the photoconductive switching pioneered by Auston et al. in the 1970s (Auston, 1975). For a more complete review of terahertz technology, its generation and its applications, the inclined reader is referred to the excellent articles of (Mittleman, 2003), (Sakai, 2005) and (Siegel, 2002).

In this section we will introduce a terahertz time domain spectrometer based on photoconductive switches driven by a Ti:Sa femtosecond laser. First, the single elements will be discussed followed by an explanation of the full spectroscopy system.

3.1 Ti:Sa femtosecond lasers

The centerpiece of a Ti:Sa femtosecond laser is a titan doped alumina crystal, which acts as the active medium inside a Fabry-Perot cavity. The crystal is driven by a diode pumped solid state laser, for example a neodymium-doped yttrium orthovanadate (ND:YVO₄) laser which emits at 532 nm and is commercially available with output powers exceeding 5W. This green light emission is well suited for pumping as it coincides with the absorption peak of the Ti:Sa crystal (see Fig. 6 right hand side). In this configuration a relaxation process inside the Ti:Sa leads to a monochromatic, continuous wave emission of the highest gain mode in the Ti:Sa gain region between 700 and 900 nm.

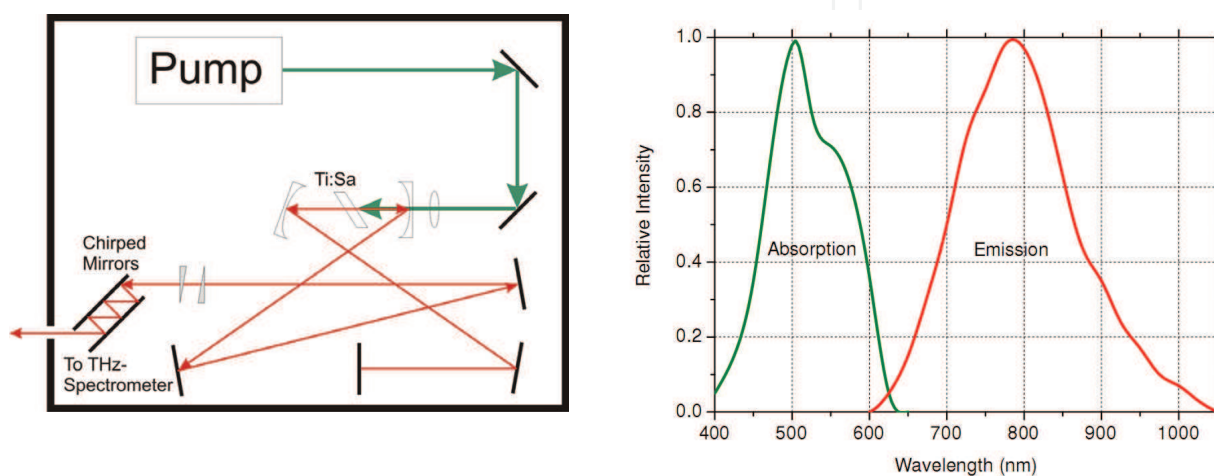


Fig. 6. The schematic setup of the femtosecond Ti:Sa laser system (left) and a sketch of the emission and absorption spectrum of the Ti:Sa crystal (right).

To obtain the desired femtosecond pulses, many modes inside the gain region have to be synchronously excited with a fixed phase relation - they have to be "mode locked". Often the Kerr-lens effect, also known as self focusing, is exploited to obtain this behaviour: For higher intensities, the laser pulse becomes strongly focused inside the crystal leading to a better overlap with the pump beam leading to an enhanced stimulated emission. Hence, pulsed emission becomes the favoured state of operation (Salin et al., 1991), (Piche & Salin, 1993). The mode locking can be induced by the artificial introduction of intensity fluctuations, e.g. by exciting the resonator end mirror with a mechanical impulse and the repetition rate of the laser can be adjusted by selecting the appropriate resonator length.

The left hand side Fig. 6 shows a sketch of a Ti:Sa laser. The green pump light is focused into the Ti:Sa crystal mounted inside the resonator. After the out coupling mirror at one end of the cavity, a dispersion compensation system, consisting of chirped mirrors is located. This additional component becomes a necessity due to the ultra short nature of the optical pulses. With a typical 60 nm spectral bandwidth around the central wavelength of 800 nm, sub-30 fs pulses result. Such pulses are extremely broadened when transmitted through dispersive media, e.g. glass lenses or other optical components. The chirped mirrors have an anomalous dispersive behaviour, pre-compensating for the normal dispersion inside the optical components after the laser, so that bandwidth limited pulses are obtained at the terahertz emitter and detector, respectively.

3.2 Photoconductive terahertz antennas

As previously mentioned, in this brief overview of terahertz spectroscopy we will focus on photoconductive antennas, also called Auston switches, as terahertz emitters and detectors (Auston, 1975), (Auston et al., 1984), (Smith et al., 1988). They consist of a semiconducting substrate with metal electrodes on top and a pre-collimating high resistivity silicon (HR-Si) lens mounted on the backside (Van Rudd & Mittleman, 2002). Though sharing the same basic structure, receiver and transmitter antenna differ in their requirements to the electrode geometry, substrate material and biasing voltage (Yano et al., 2005).

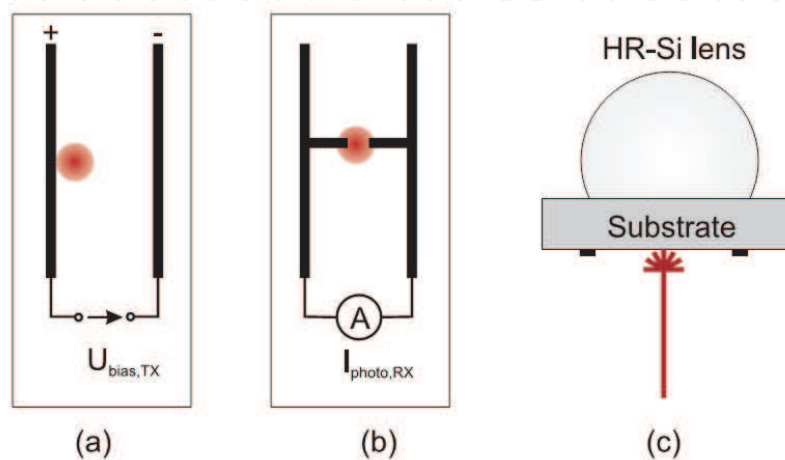


Fig. 7. Metallization structure of a stripline antenna (a) and a dipole antenna (b). The antenna mounted onto the collimating lens (c).

In case of the transmitter antenna, GaAs or low temperature grown GaAs (LT-GaAs) are commonly used as semiconducting substrates. The electrode geometry varies in different designs and can be custom-tailored to the application. A parallel strip line or a bowtie configuration is common. The electrodes are connected to a DC-bias voltage source and the laser spot is focused near the anode (Ralph & Grischkowsky, 1991). When a laser pulse hits the substrate, free carriers are generated and immediately separated in the bias field, giving rise to a photocurrent. The Drude model yields, that the electric THz field emitted, is directly proportional to the time derivative of the photocurrent. If the carrier scattering, relaxation and recombination times of the substrate are known, the behaviour of the transmitter can be accurately simulated (Jepsen et al., 1996).

The substrate of the receiver antenna is made of LT-GaAs which has arsenic clusters as carrier traps that ensure a short carrier lifetime. The electrodes usually have the form of a Hertzian dipole as illustrated in Fig. 7. The laser is focused into the gap between the electrodes. When the laser pulse hits the substrate, the generated carriers short the photoconductive gap and the electric field of the incoming THz pulse separates the free carriers, driving them towards the electrodes. Thus, a current can be detected which is a measure of the average strength of the electric THz field over the lifetime of the optically generated carriers. Due to the LT-GaAs substrate, the life time of the carriers is very short compared to the length of the terahertz pulse. Thus the approximation that only one point in time of the terahertz pulse is sampled can be made.

3.3 A terahertz time domain spectrometer

Now that we have discussed the single elements of a terahertz spectroscopy system (emitter, detector and femtosecond laser source) we shall investigate a complete terahertz time domain spectrometer as shown in Fig. 8.

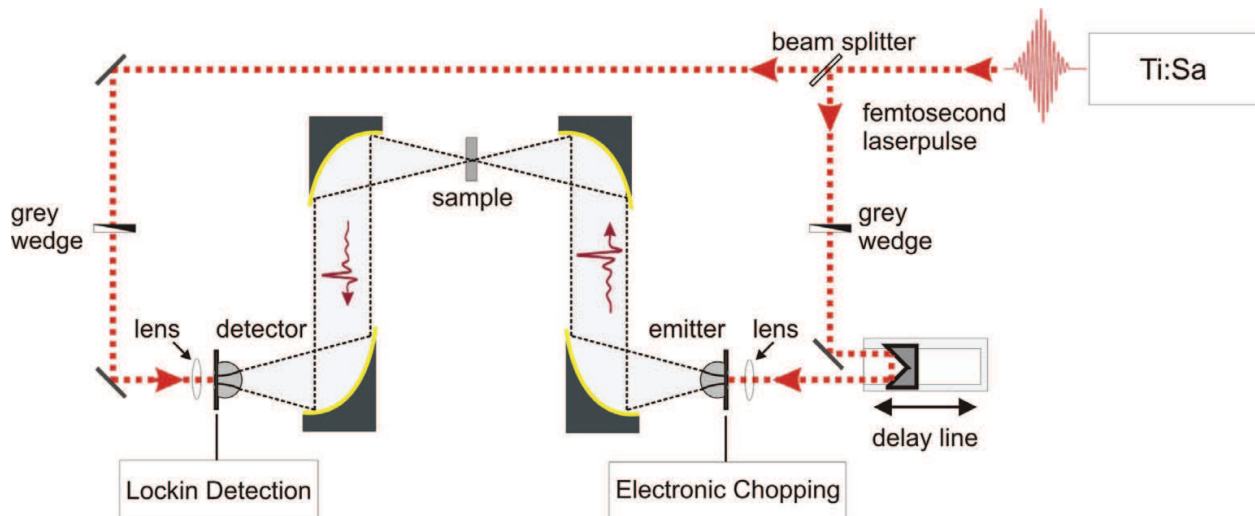


Fig. 8. Basic structure of a THz-TDS system.

The femtosecond laser pulse, generated by the Ti:Sa laser, is divided into an emitter and a detector arm inside a beam splitter. Grey wedges are used to set the desired power level and lenses focus the laser beams onto the photoconductive antennas. The terahertz radiation is guided by off-axis parabolic mirrors (OPMs). In order to analyze small-sized samples, the OPMs are used to create an intermediate focus, which is typically of the size of a few millimeters. In the emitter arm, a motorized delay line varies the time at which the laser pulse creates the terahertz radiation inside the photoconductive transmitter with respect to the time that the photoconductive receiver is gated. Thus, by varying the optical delay, the terahertz pulse is sampled step by step. A typical terahertz pulse with the corresponding Fourier spectrum obtained in such a spectrometer is depicted in Fig. 9.

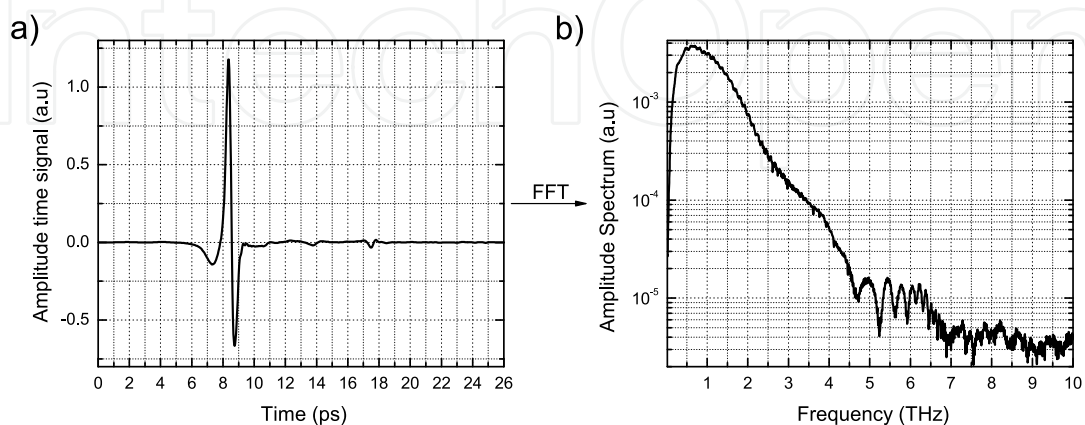


Fig. 9. Typical time domain signal (left) and the corresponding spectrum (right).

3.4 Material parameter extraction with terahertz time domain spectroscopy

Due to the coherent detection scheme of terahertz time domain spectroscopy, both phase and amplitude information of the electric field can be accessed. This circumstance enables the direct extraction of the complex refractive index $\underline{n} = n - i\kappa$ without the need for the Kramers-Kronig relations as required in the case of FIR spectroscopy. Here, n is the real part of the refractive index and κ the extinction coefficient. From these two measures the complex permittivity $\underline{\varepsilon}_r = \varepsilon_r' - i\varepsilon_r''$ with the real part $\varepsilon_r' = n^2 - \kappa^2$ and the imaginary part $\varepsilon_r'' = 2n\kappa$ as well as the absorption coefficient $\alpha = 2k_0\kappa$ can be determined. $k = \frac{\omega}{c_0}$ denotes the free space angular wave number, ω the angular frequency and c_0 the speed of light in free space.

The basic idea of material parameter extraction from THz TDS data is the comparison of a sample and a reference pulse, once with and once without the sample mounted in the terahertz beam. In most approaches the Fourier spectra of both pulses are calculated and a transfer function is defined as the complex quotient of the sample spectrum to the reference spectrum. Different algorithms for the data analysis were developed. Most recently a new approach, which enables the simultaneous identification of the refractive index n , the absorption coefficient α and the sample thickness even in case of ultra thin samples in the sub 100 μm regime has been proposed (Scheller et al. 2009, b). As this approach was employed for the material parameter extraction of most datasets presented in this chapter we shall now briefly review its basic working principle.

The first step in the data extraction is the formulation of a general theoretic transfer function for the sample under investigation depending on the refractive index n , the absorption coefficient α , and the sample thickness L . In order to create such a transfer function the number of multiple reflections M which occur during the measured time window is determined in a preprocessing step which assumes an initial thickness L_0 . The basic shape of the theoretical transfer function is given by

$$H(\omega) = A_0 \exp\left(-i \frac{\omega}{c_0} (\underline{n} - 1) \cdot D\right) + A_1 \exp\left(-i \frac{\omega}{c_0} (3\underline{n} - 1) \cdot D\right) + \dots \quad (18)$$

where A_i is given as the i^{th} of M elements that are functions of the Fresnel coefficients. In a following step, an error function defined by the difference of the theoretical transfer function and the measured one is minimized which yields n and α as functions of the sample thickness L . To unambiguously derive n , α and the material thickness L , the Fabry-Perot oscillations superimposed to the measured material parameters have to be considered. Hence, an additional Fourier transform is applied to the frequency domain material parameters which transforms the superimposed Fabry-Perot oscillations to a discrete peak in the so called quasi space regime. Now the correct sample thickness as well as n and α can be determined by minimizing the peak amplitude completing the material parameter extraction.

As a demonstration of this technique, we analyse a 54.5 μm silicon wafer. If the correct thickness is chosen the peak values are minimized. Fig. 10 a) shows the refractive index n for different thicknesses over the frequency. For the correct thickness determined from the quasi space peak minimization (Fig. 10 b)), the Fabry Perot oscillations vanish from the material parameter spectra

The inclined reader finds a detailed discussion of this algorithm in (Scheller et al., 2009, b).

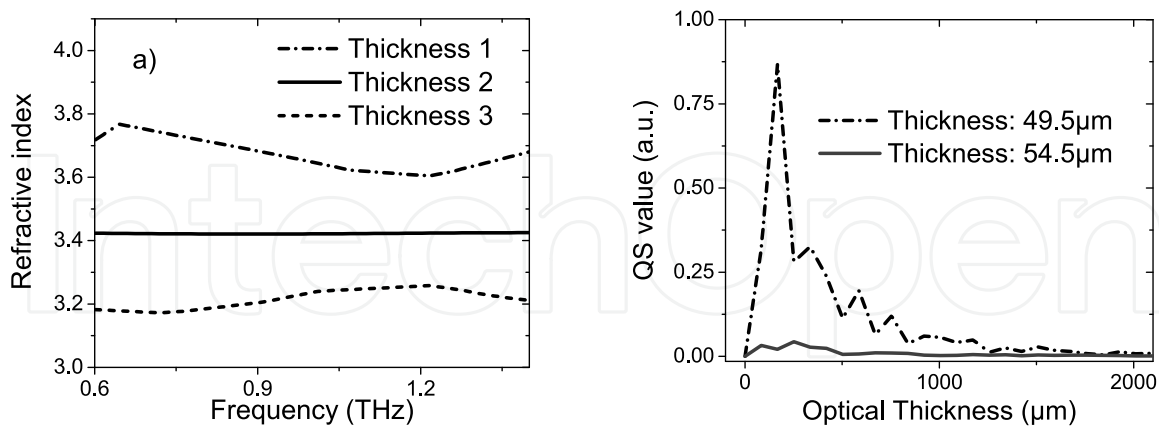


Fig. 10. The extracted refractive index for different thicknesses (a) and the corresponding QS values (b).

4. Application scenarios

4.1 Polymeric compounds

To evaluate the applicability of the different EMTs, we shall now investigate three additive concentration series of polymeric compounds, comparing measurement and simulation results of the refractive index at 1 THz (Scheller et al., 2009, a). The additive particle sizes are less than 5 μm so that scattering effects should remain negligible. Hence, a quasi-static effective medium theory fully describes the dielectric behaviour of the composites at the wavelength of interest. The samples consist of injection-molded rods of 1 mm to 3 mm thickness. The additives differ both in shape and permittivity. After THz TDS measurements, the additive concentration was confirmed by combustion, determining the ignition residue content of the compounds. The measurement setup consists of a transmission terahertz time domain spectrometer as described in section 3.

The first series of samples comprises magnesium hydroxide $\text{Mg}(\text{OH})_2$ -filled low-density polyethylene (LLDPE) together with a compressed pellet of pure $\text{Mg}(\text{OH})_2$, which was used to quantify the 100% additive content permittivity value. Utilizing the LLL model, this value was extrapolated from the measurement result of the porous pellet. Nelson et al. demonstrated that this procedure delivers accurate results for granular and powdered materials (Nelson, 2005). The $\text{Mg}(\text{OH})_2$ particles have a hexagonal disc-like shape. Calculations employing the effective medium theories are compared to the measured data in Fig. 11. While the EB and the PvS model deliver good agreement with the measured data, the MG approaches show a significant discrepancy to the experimentally obtained results. This circumstance can be explained by the fact that the MG model only considers spherical particles while both the EB and the PvS model are shape-dependent. The predicted values based on the LLL theory, which does not consider any particle shape, cannot reach the accuracy of either the EB or the PvS calculations but performs better than the MG theory in case of this material system. The CRIs equation's prediction additionally exhibits a good agreement to measured data but lacks any physical motivation.

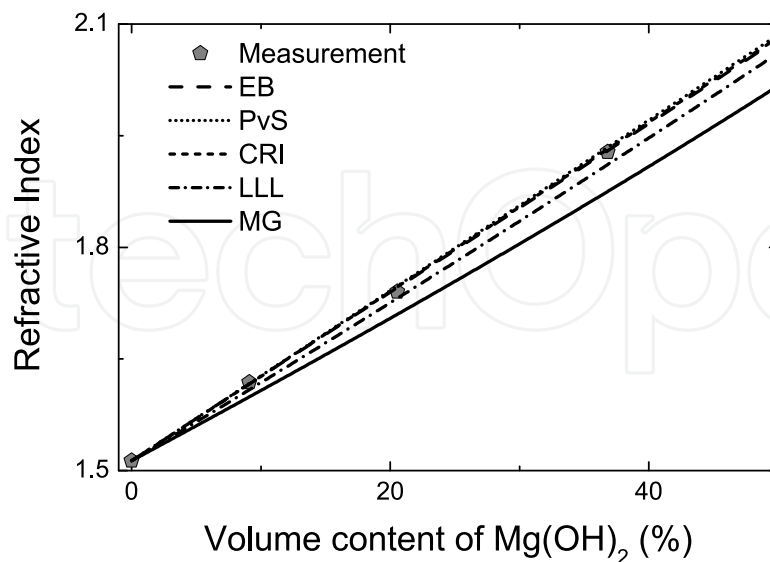


Fig. 11. The refractive index of the Mg(OH)₂ compound system for different volumetric contents of the additives compared to the EMT's predictions.

The second series consists of rutile titania (TiO₂) particles embedded in a polypropylene (PP) host matrix. In this case, the 100% additive volume content value was directly extracted from a rutile crystal. Both, measurements along the fast and the slow axis of the birefringent rutile titania crystal were conducted and a weighted average of the permittivity was determined. The obtained material parameters of the crystal are shown in Fig. 12.

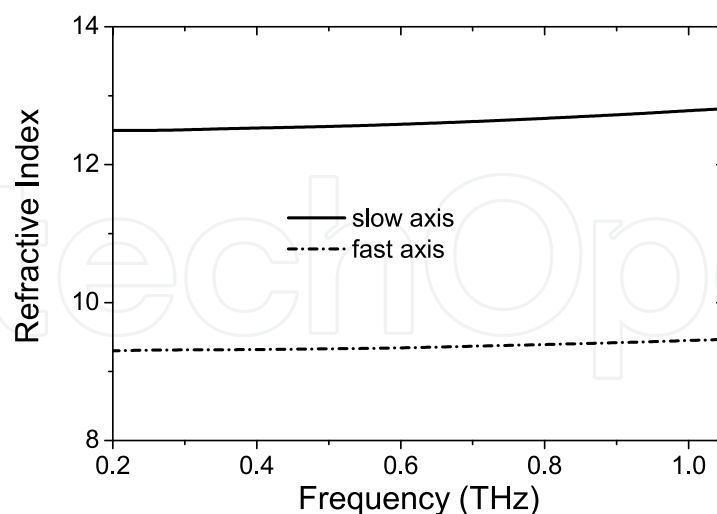


Fig. 12. The refractive index of the fast and the slow axis of a rutile crystal.

This step was necessary, as the LLL model, used for the extraction of the 100% additive values from the compressed pellets in case of the other material systems, is unable to properly describe the behaviour of the TiO₂-air mixture due to the large dielectric contrast.

As a Taylor approximation is contained in the LLL models derivation, valid predictions cannot be expected in this case. Apart, from the LLL and the CRI model, all other existing theories should be well suited to accurately describe the behaviour of this material system as long as only diluted mixtures are considered. An interesting aspect of this material system is the high permittivity contrast between the additive and the host combined with the spherical particle shape, which allows to clearly evaluate the capabilities of each approach.

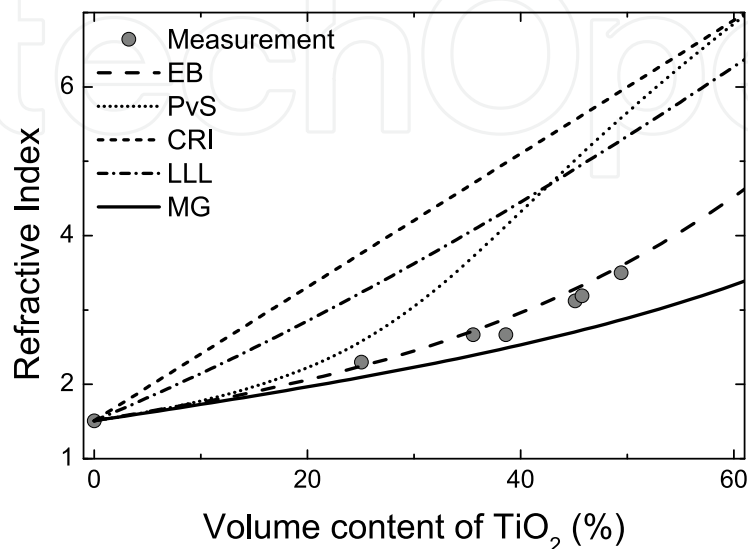


Fig. 13. The measured results of the TiO₂-PP mixture compared to the predictions of the different models.

The measured data together with the values predicted from the theories are shown in Fig. 13. As expected, all models, except the LLL and the CRI, deliver similar results as long as only low particle concentrations below 15 volume percent are considered. For higher concentrations, only the EB theory can still accurately model the mixture behaviour. While the MG theory delivers much smaller permittivity values compared to the measurements, the PvS model deviates in the opposite direction. The LLL and the CRI model do not yield a good estimation of the measured permittivity for any additive concentration due to the reasons discussed above.

The last series of samples which we will consider here comprises calcium carbonate (CaCO₃)-filled polypropylene samples. Analogous to the Mg(OH)₂-series, a compressed pure additive pellet of CaCO₃ was employed to extract the 100% additive content permittivity value. The CaCO₃ particles exhibit a cubic shape. Cubes are one of the few shapes that cannot be described as ellipsoids. In addition, the aspect ratio of the cuboids under investigation is not uniform. However, by considering a distribution of different aspect ratios, the PvS and the EB model should be able to reach a performance close to the modelling with the actual particle shape.

Calculations based on the physical models and the measured permittivity are illustrated in Fig. 14. For the EB and the PvS model, a rectangular distribution of aspect ratios between the longer and the shorter axis is assumed. While the EB and PvS model well describe the measured behaviour, closely followed by the LLL and the CRI approach, the MG theories

suggest permittivity values that strongly deviate from the experimentally determined material parameters.

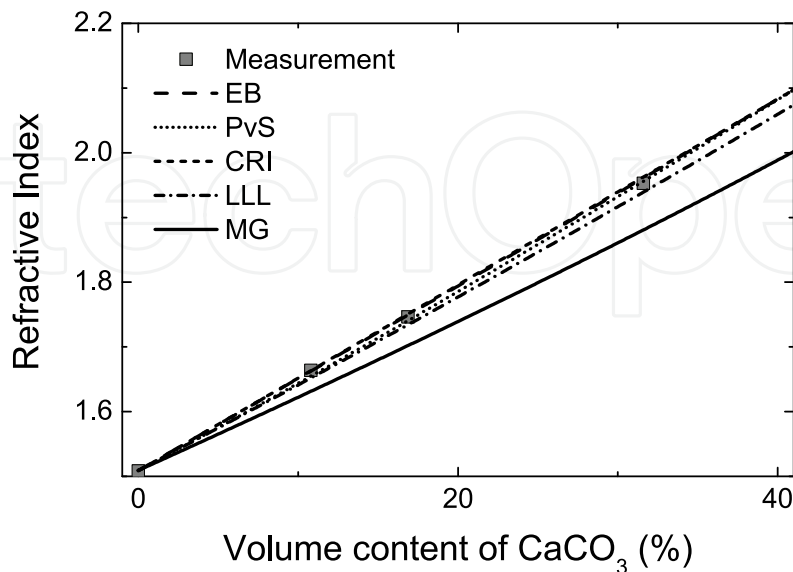


Fig. 14. The measured results of the CaCO₃ system compared to the predictions of the different models.

These results indicate, that the PvS and the EB model offer most flexibility and are sufficient for most applications. However, if the contrast in permittivity is small and the mixture consist of anisotropic shaped particles, the relation between the volumetric content and the refractive index exhibit a close to linear behaviour, allowing to utilize the CRI equation to estimate the resulting permittivity. The LLL model delivers good results for two of the three cases and is applicable if no high contrast in permittivity occurs and can be seen as a good choice if no information about the particle shape is known or if the mixture consists of irregularly shaped components.

4.2 Hydration monitoring of plant leaves

Hydration monitoring of leaves is of high importance for farmers and plant physiologists alike. It can provide valuable information about irrigation management and helps to control drought stress. THz radiation is ideally suited for studying the water content in leaf tissue due to the strong water induced absorption present at THz frequencies (Hadjiloucas et al., 1999). However, a physical modeling is required to create a connection between the measured data and the water content of the leaves.

A leaf can be described as a multi compound mixture, that mainly consists of the following three parts: air, water, and the solid plant material. Therefore, an EMT is in principal suitable to model the dielectric constant of this biological sample. Due to the irregular structure of the leaf, the LLL model is suitable to solve this specific problem. However, LLL is just able to compute the effective permittivity of a compound consisting of two components so that an extension has to be made in order to match these enhanced requirements. Such a third order extension

$$\sqrt[3]{\epsilon_R} = f_W \sqrt[3]{\epsilon_W} + f_S \sqrt[3]{\epsilon_S} + (1 - f_W - f_S) ,$$

where f_i is the concentration of the components is essential to account for the three parts of the leaf. The index W and S refers to the water and the solid plant material, respectively.

A series of fresh and water stressed *Coffea arabica* leaves was measured in a TDS setup by Jördens at coworkers (Jördens et al., 2009, a). Afterwards the leaves were detached from the plant, the thickness and mass was measured and the water was pressed out. The concentration of water, air, and solid plant material can be determined with the information of the thickness and the mass of each leaf before and after pressing.

The dielectric properties of the solid plant material were identified by TDS measurements on the pressed and dried leaves. The pure water permittivity was calculated by a dual Debye model analogue to (Liebe et al., 1991). As can be seen in Fig. 15, the water exhibits an intense anomalous dispersion. Thus, a similar behavior is expected for the optical parameters of the leaf.

The measured refractive index and the absorption of two leaves, one fresh and one stressed, are shown in (Fig. 16) together with the model's predictions. As the refractive index of water exceeds the ones of the other mixtures components, the resulting refractive index of the leaves is higher for larger water content. Over the whole spectral range, a good agreement between the simulated and measured results is obtained, indicating the applicability of the THz technology in combination with EMTs to monitor the hydration status of plants

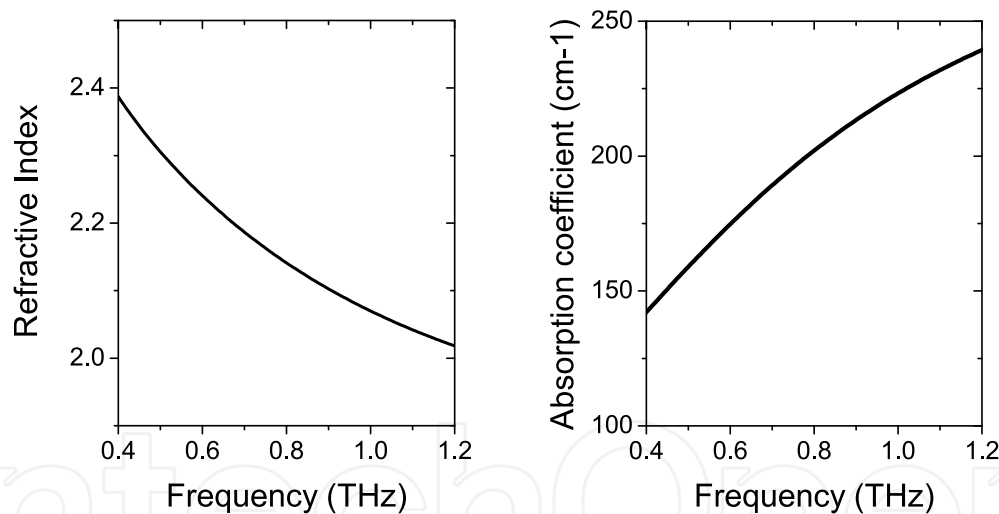


Fig. 15. The refractive index and the absorption coefficient of water at 20 °C calculated from the Debye model.

4.3 Isotropic material mixtures

In the case of the application scenarios described above anisotropic mixtures were considered. Yet, if the particles within the mixture exhibit an isotropic shape, an orientation of these will induce a macroscopic birefringence of the effective medium. As one example we will shortly examine a system of glass fibres filled HDPE. Due to the injection molding production process, a notable orientation of the fibres inside the direction of the mold flow is expected. Consequently, the refractive indices parallel and perpendicular to this direction will differ as a consequence of the isotropic material system.

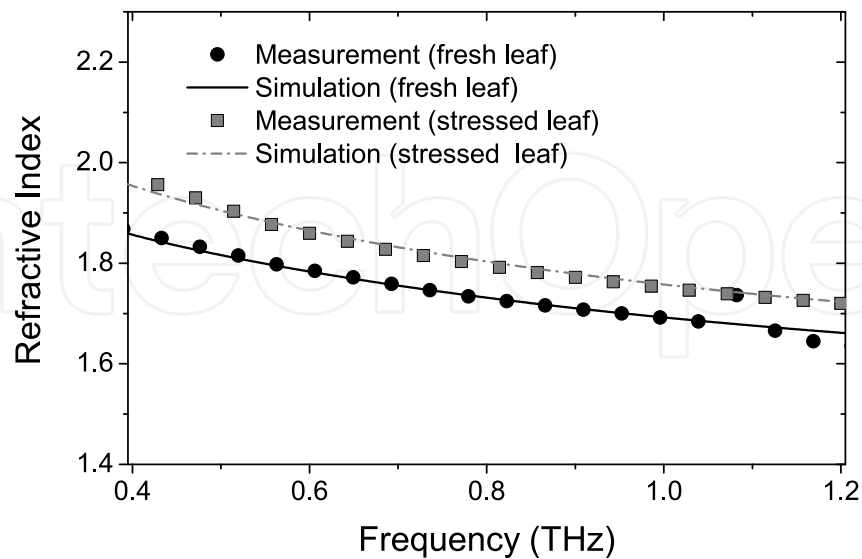


Fig. 16. Measured and simulated refractive index of a fresh and a stressed *Coffea arabica* leaf.

The PvS model was chosen to analyze the resulting effective medium, because the permittivity contrast between the HDPE and the borosilicate based fibres is small and the refractive indices along the different orientations can be calculated directly by Eq. 8, assuming rod like particles within the matrix. The resulting refractive indices are shown in Fig. 17 together with measured values, obtained from a 3 mm thick fibre enforced polymer.

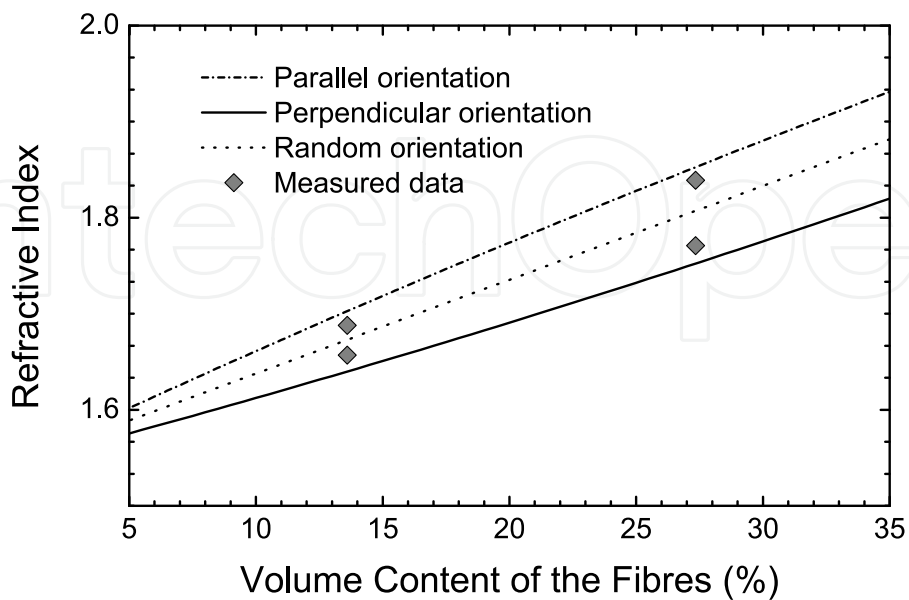


Fig. 17. The simulated refractive indices of the glass fibre - HDPE composite at 400GHz

A distinctive birefringence can be observed in the simulation. The measured data exhibit a slightly lower one. This discrepancy can be explained by a non uniform orientation of the particles. If only the majority of the fibres are orientated along the mold flow direction, the resulting birefringence will deviate from the maximum values. As a consequence, THz measurements can be utilized to determine the fibres content of the mixture and their degree of orientation simultaneously (Jördens et al., 2009, b).

5. Conclusion and outlook

In this chapter a short introduction into a selection of quasi static effective medium theories was presented. Their potential and restrictions were illuminated by a choice of representative application scenarios ranging from polymeric compounds to biological samples. However, the relatively long wavelengths of the terahertz waves enables for a wide applicability within this frequency range without the necessity of including volumetric scattering effects in the calculations. Therefore, an accurate analytical modelling of various problems can be achieved utilizing such EMTs. The Table 2 gives a short overview of exemplary application scenarios and the EMTs of choice.

| Application Scenario | EMT of choice | |
|---|---------------|--|
| Mixtures with high contrast in permittivity, spherical particles | EB | |
| Mixtures with high contrast in permittivity, ellipsoidal particles | EB, PvS | |
| Mixtures with low contrast in permittivity, irregular or unknown shaped particles | LLL, CRI | |
| Mixtures of powders, porous pellets | LLL, CRI | |
| Mixtures consisting of isotropic components | EB, PvS | |

Table 2. Overview of typical application scenarios for the EMTs mentioned in the text.

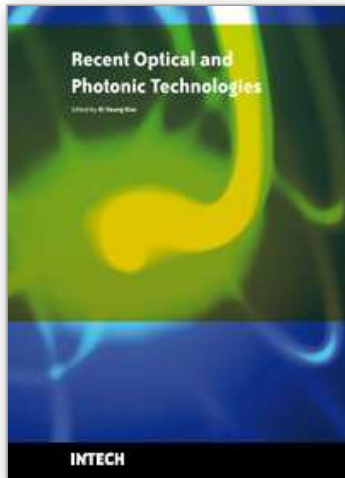
6. References

- Auston, D. H. (1975). Picosecond optoelectronic switching and gating in silicon, *Applied Physics Letters*, AIP, 1975, 26, 101-103
- Auston, D. H.; Cheung, K. P.; Smith, P. R. (1984). Picosecond photoconducting Hertzian dipoles, *Applied Physics Letters*, AIP, 1984, 45, 284-286
- Banhegyi, G. (1986). Comparison of electrical mixture rules for composites. *Colloid Polym. Sci.*, Vol. 264, 1986, 1030-50
- Beard, M. C; Turner, G.M.; Schmuttenmaer, C. A. (2002). Size-Dependent Photoconductivity in CdSe Nanoparticles as Measured by Time-Resolved Terahertz Spectroscopy. *Nano Letters*, Vol. 2 2002, 983-987
- Böttcher, C. J. (1942). Zur Theorie der inneren elektrischen Feldstärke. *Physica*, Vol. 9, No. 10, 1942, 937-943

- Bruggeman, D. (1935). Berechnung verschiedener physikalischer Konstanten von heterogenen Substanzen: I Dielektrizitätskonstanten und Leitfähigkeiten der Mischkörper aus isotropen Substanzen. *Annalen der Physik*, Vol. 24, 1935, 636-664
- Hadjiloucas, S.; Karatzas, L. S.; Bowen, J. W. (1999). Measurements of leaf water content using terahertz radiation. *IEEE Transactions on microwave theory and techniques*, Vol. 47, No. 2, 1999, 142-149
- Hendry, E.; Koeberg, M.; O'Regan B.; Bonn M. (2006). Local Field Effects on Electron Transport in Nanostructured TiO₂ Revealed by Terahertz Spectroscopy. *Nano Letters*, Vol. 6, 2006, 755-759
- Jackson, J. D. (1999). *Classical electrodynamics*, Wiley & Sons, Inc, 047130932X, New York
- Jepsen, P. U.; Jacobsen, R. H.; Keiding, S. R. (1996). Generation and detection of terahertz pulses from biased semiconductor antennas, *J. Opt. Soc. Am. B*, 1996, 13, 2424-2436
- Jördens, C.; Scheller, M.; Breitenstein, B.; Selmar, D.; Koch, M. (2009, a). Evaluation of the Leaf Water Status by means of the Permittivity at Terahertz Frequencies. *Journal of Biological Physics*, 2009, 35, 255-264
- Jördens, C.; Scheller, M.; Wietzke, S.; Romeike, D.; Jansen, C.; Zentgraf, T.; Wiesauer, K.; Koch, M. (2009, b). Terahertz spectroscopy to study the orientation of glass fibres in reinforced polymers. *Submitted to Composite Science and Technology*, 2009
- Kimmit, M. (2003). Reststrahlen to T-Rays - 100 Years of Terahertz Radiation, *Journal of Biological Physics*, 2003, 29, 77-85
- Kittel, C. (1995). *Introduction to solid state physics*, Wiley & Sons, Inc, 0471111813, New York
- Kuebler, C.; Huber, R.; Leitenstorfer, A. (2005). Ultrabroadband terahertz pulses: generation and field-resolved detection, *Semiconductor Science and Technology*, 2005, 20, S128-S133
- Levy, U.; Abashin, M.; Ikeda, K.; Krishnamoorthy, A.; Cunningham, J.; Fainman, Y. (2007). Local Field Effects on Electron Transport in Nanostructured TiO₂ Revealed by Terahertz Spectroscopy. *Physical Review Letters*, Vol. 98, 2007, 243901
- Liebe, H. J.; Hufford, G. A.; Manabe, T. (1991). A model for the complex permittivity of water at frequencies below 1 THz. *International Journal of Infrared and Millimeter Waves*, Vol. 12, No. 7, 1991, 659-675
- Looyenga, H. (1965). Dielectric constants of heterogeneous mixtures. *Physica*, Vol. 31, 1965, 401-406
- Maxwell-Garnett, J. C. (1904). Colours in metal glasses and in metallic films. *Philosophical Transactions of the Royal Society of London. Series A*, Vol. 203, 1904, 385-420
- Mittleman (ed.), D. (2003). *Sensing With Terahertz Radiation*, Springer-Verlag, Berlin, 2003
- Moulton, P. F. (1986). Spectroscopic and laser characteristics of Ti:Al₂O₃, *J. Opt. Soc. Am. B*, OSA, 1986, 3, 125-133
- Nelson, S. O.; You, T. S. (1990). Relationships between microwave permittivities of solid and pulverised plastics. *J. Phys. D: Appl. Phys.*, Vol. 9, No. 10, 1990, 346-353
- Nelson, S. O. (2005). Density-permittivity relationships for powdered and granular materials. *IEEE Transactions on Instrumentation and Measurement*, Vol. 54, No. 5, 2005, 2033-2040
- Piche, M.; Salin, F. (1993). Self-mode locking of solid-state lasers without apertures, *Opt. Lett.*, OSA, 1993, 18, 1041
- Polder, D.; van Santen, J. H. (1946). The effective permeability of mixtures of solids. *Physica*, Vol. No. 12, 5, 1946, 257-271

- Ralph, S. E.; Grischkowsky, D. (1974). Trap-enhanced electric fields in semi-insulators: The role of electrical and optical carrier injection, *Applied Physics Letters, AIP*, 1991, 59, 1972-1974
- Sakai (ed.), K. (2005). Terahertz Optoelectronics, *Springer Berlin*, 2005
- Salin, F.; Squier, J.; Piché, M. (1991). Mode locking of Ti:Al₂O₃ lasers and self-focusing: a Gaussian approximation, *Opt. Lett., OSA*, 1991, 16, 1674-1676
- Scheller, M.; Wietzke, S.; Jansen, C.; Koch, M. (2009, a). Modelling heterogeneous dielectric mixtures in the terahertz regime: a quasi-static effective medium theory. *J. Phys. D: Appl. Phys.*, Vol. 42, 2009, 065415
- Scheller, M.; Jansen, C.; Koch, M. (2009, b). Analyzing sub-100- μm samples with transmission terahertz time domain spectroscopy. *Optics Communications*, Vol. 282, 2009, 1304-1306
- Siegel, P. H. (2002). Terahertz technology, *IEEE Trans. on MTT*, 2002, 50, 910-928
- Smith, P.; Auston, D.; Nuss, M. (1988). Subpicosecond photoconducting dipole antennas, *IEEE Journal of Quantum Electronics*, 1988, 24, 255-260
- Van Rudd, J; Mittleman, D. M. (2002). Influence of substrate-lens design in terahertz time-domain spectroscopy, *Journal of the Optical Society of America B: Optical Physics, OSA*, 2002, 19, 319-329
- Yano, R.; Gotoh, H.; Hirayama, Y.; Miyashita, S.; Kadoya, Y. & Hattori, T. (2005). Terahertz wave detection performance of photoconductive antennas: Role of antenna structure and gate pulse intensity, *Journal of Applied Physics, AIP*, 2005, 97, 103103

IntechOpen



Recent Optical and Photonic Technologies

Edited by Ki Young Kim

ISBN 978-953-7619-71-8

Hard cover, 450 pages

Publisher InTech

Published online 01, January, 2010

Published in print edition January, 2010

Research and development in modern optical and photonic technologies have witnessed quite fast growing advancements in various fundamental and application areas due to availability of novel fabrication and measurement techniques, advanced numerical simulation tools and methods, as well as due to the increasing practical demands. The recent advancements have also been accompanied by the appearance of various interdisciplinary topics. The book attempts to put together state-of-the-art research and development in optical and photonic technologies. It consists of 21 chapters that focus on interesting four topics of photonic crystals (first 5 chapters), THz techniques and applications (next 7 chapters), nanoscale optical techniques and applications (next 5 chapters), and optical trapping and manipulation (last 4 chapters), in which a fundamental theory, numerical simulation techniques, measurement techniques and methods, and various application examples are considered. This book deals with recent and advanced research results and comprehensive reviews on optical and photonic technologies covering the aforementioned topics. I believe that the advanced techniques and research described here may also be applicable to other contemporary research areas in optical and photonic technologies. Thus, I hope the readers will be inspired to start or to improve further their own research and technologies and to expand potential applications. I would like to express my sincere gratitude to all the authors for their outstanding contributions to this book.

How to reference

In order to correctly reference this scholarly work, feel free to copy and paste the following:

Maik Scheller, Christian Jansen, and Martin Koch (2010). Applications of Effective Medium Theories in the Terahertz Regime, Recent Optical and Photonic Technologies, Ki Young Kim (Ed.), ISBN: 978-953-7619-71-8, InTech, Available from: <http://www.intechopen.com/books/recent-optical-and-photonic-technologies/applications-of-effective-medium-theories-in-the-terahertz-regime>

INTECH
open science | open minds

InTech Europe

University Campus STeP Ri
Slavka Krautzeka 83/A
51000 Rijeka, Croatia
Phone: +385 (51) 770 447
Fax: +385 (51) 686 166

InTech China

Unit 405, Office Block, Hotel Equatorial Shanghai
No.65, Yan An Road (West), Shanghai, 200040, China
中国上海市延安西路65号上海国际贵都大饭店办公楼405单元
Phone: +86-21-62489820
Fax: +86-21-62489821

www.intechopen.com

www.intechopen.com

IntechOpen

IntechOpen

© 2010 The Author(s). Licensee IntechOpen. This chapter is distributed under the terms of the [Creative Commons Attribution-NonCommercial-ShareAlike-3.0 License](#), which permits use, distribution and reproduction for non-commercial purposes, provided the original is properly cited and derivative works building on this content are distributed under the same license.

IntechOpen

IntechOpen